Array 27 (2025) 100477

Contents lists available at ScienceDirect

Array

journal homepage: www.elsevier.com/locate/array

Ultra Wideband radar-based gait analysis for gender classification using artificial intelligence

Adil Ali Saleem [a], Hafeez Ur Rehman Siddiqui [a,*], Muhammad Amjad Raza [a], Sandra Dudley [b], Julio César Martínez Espinosa [c,d,g], Luis Alonso Dzul López [c,d,e,f,h], Isabel de la Torre Díez [i]

[a] Institute of Computer Science and Information Technology, Khwaja Fareed University of Engineering and Information Technology, Rahim Yar Khan, 64200, Punjab, Pakistan
[b] Bioengineering Research Centre, School of Engineering, London South Bank University, 103 Borough Road, London, SE1 0AA, United Kingdom
[c] Universidad Europea del Atlántico, Isabel Torres 21, Santander, 39011, Spain
[d] Universidad Internacional Iberoamericana, Campeche, 24560, Mexico
[e] Universidad Internacional Iberoamericana, Arecibo, 00613, USA
[f] Universidade Internacional do Cuanza, Cuito, Bié, Angola
[g] Universidad de La Romana, La Romana, Dominican Republic
[h] Fundación Universitaria Internacional de Colombia, Bogotá, Colombia
[i] Department of Signal Theory, Communications and Telematics Engineering, University of Valladolid, 47011, Valladolid, Spain

ARTICLE INFO

Keywords:
Gait
Ultra-wide band radar
Gender classification
Spectral features
Feed forward artificial neural network
Ridge classifier
Hist gradient boosting

ABSTRACT

Gender classification plays a vital role in various applications, particularly in security and healthcare. While several biometric methods such as facial recognition, voice analysis, activity monitoring, and gait recognition are commonly used, their accuracy and reliability often suffer due to challenges like body part occlusion, high computational costs, and recognition errors. This study investigates gender classification using gait data captured by Ultra-Wideband radar, offering a non-intrusive and occlusion-resilient alternative to traditional biometric methods. A dataset comprising 163 participants was collected, and the radar signals underwent preprocessing, including clutter suppression and peak detection, to isolate meaningful gait cycles. Spectral features extracted from these cycles were transformed using a novel integration of Feedforward Artificial Neural Networks and Random Forests , enhancing discriminative power. Among the models evaluated, the Random Forest classifier demonstrated superior performance, achieving 94.68% accuracy and a cross-validation score of 0.93. The study highlights the effectiveness of Ultra-wideband radar and the proposed transformation framework in advancing robust gender classification.

1. Introduction

Gender classification plays an essential role in human–computer interaction [1]. Automated gender detection is a modern technique that revolutionizes the process of identifying a person's gender, with far-reaching implications in numerous academic and practical fields. Integrating gender recognition into contemporary authentication procedures improves security and biometrics [2], thereby strengthening identity verification in access control and surveillance systems. In the complex field of human–computer interaction [1], automatic gender identification optimizes usability and interaction by personalizing user experiences based on gender-specific preferences. Gender differentiation in the dynamic landscape of mobile applications [3] refines user profiling by tailoring content and features to gender-specific preferences, thereby enhancing user engagement. Digital forensics [4] uses automatic gender detection to unearth nuanced insights, enriching investigations by interpreting gender signals in multimedia artifacts. Consumer research [5] benefits from gender classification's profound insights, strategically tailoring marketing strategies to gender-specific behaviors. Behavioral analysis [6] thrives on gender-based patterns, enhancing our comprehension of the complex relationship between gender and behavior. Automated gender detection has a significant impact on personalization and recommender systems [7], enhancing recommendations, services, and content curation to correspond with users' gender-related preferences and, ultimately, increasing user satisfaction.

* Corresponding author.
E-mail addresses: adilalisaleem@gmail.com (A.A. Saleem), Hafeez@kfueit.edu.pk (H.U.R. Siddiqui), Ch.AmjadRaza@gmail.com (M.A. Raza), dudleyms@lsbu.ac.uk (S. Dudley), julio.martinez@unini.edu.mx (J.C.M. Espinosa), luis.dzul@unini.edu.mx (L.A.D. López), itordie@gmail.com (I. de la Torre Díez).

https://doi.org/10.1016/j.array.2025.100477
Received 17 June 2025; Received in revised form 15 July 2025; Accepted 23 July 2025
Available online 4 August 2025

This multifaceted concept has implications in the fields of security, human–computer interaction, mobile applications, digital forensics, consumer research, behavioral analysis, and personalization systems. As discourse evolves, the convergence of gender classification and technology continues to refine interactions, with reverberations in numerous disciplines. However, many of these applications demand contactless, privacy-preserving, and robust sensing solutions characteristics that conventional visual or wearable systems often fail to deliver.

Biometric methods for determining human gender include facial recognition [8–10], handwriting analysis [4,11], body posture [12], speech recognition [13–18], and gait analysis [19–23]. Among these, facial and gait-based features are widely used for gender classification, and are also relevant to tasks such as identity verification, age estimation, and emotion recognition [24]. While high-resolution facial imagery can yield high classification accuracy, challenges arise in practical scenarios where faces are partially occluded or captured from a distance, resulting in low-quality data unsuitable for accurate detection [25]. Gait-based methods offer a promising alternative as they do not rely on high-resolution imagery and can operate at a distance. Gait refers to the unique walking pattern of individuals [24] and can be recorded using various modalities, including vision-based and wearable sensor systems. However, the effectiveness of vision-based methods may depend heavily on factors such as camera quality, lighting, and viewing angles [26]. Similarly, wearable sensor systems such as those using accelerometers, gyroscopes, and pressure sensors may introduce noise due to sensor placement variability or user discomfort, which can affect signal quality and model performance [27]. These considerations motivate the exploration of alternative sensing technologies that offer contactless, privacy-preserving, and robust data acquisition under diverse conditions.

In this research, a unique strategy is proposed to address these issues by employing gait analysis with Ultra-Wideband (UWB) radar for gender classification. Although UWB radar has applications in gait analysis [23,28–35], its use for gender classification in conjunction with gait analysis represents a novel and unexplored field. Using UWB radar technology, this approach analyzes the distinct gait patterns of individuals in order to determine their gender. In contrast to conventional systems, UWB radar emits very short electromagnetic pulses. This unique characteristic gives the radar unmatched precision, allowing it to detect even the most intricate movement variations. Notably, UWB radar is capable of penetrating obstacles such as garments, thereby eliminating the need for direct line-of-sight observations [36]. This characteristic is especially advantageous in real-world situations where obstructions and environmental factors can affect data collection. These properties make UWB radar particularly suitable for sensitive environments such as healthcare facilities, secured buildings, or smart homes, where accurate gender classification must occur under occlusion, poor lighting, or strict privacy requirements. Despite its advantages, UWB radar can be sensitive to clutter and interference, and may face challenges in distinguishing individuals in multi-user environments. These limitations warrant further investigation for practical deployment.

1.1. Research contributions

This manuscript presents novel research with the following specific and impactful contributions:

- This investigation examines the efficacy of Ultra-Wideband (UWB) radar technology in identifying gender-specific gait pattern differences. A novel and substantial radar dataset was compiled from a cohort of 163 KFUEIT volunteers (88 males, 75 females), making it one of the largest radar-based gait datasets for gender classification, particularly within the Pakistani demographic.
- To optimize gender classification accuracy and enhance data quality, a series of customized preprocessing techniques were employed. These include a three-pulse canceller (Eq. (1)) for effective clutter removal and an adaptive, two-threshold peak detection technique (Eq. (2)) developed specifically for robust gait cycle segmentation from UWB radar signals.
- A novel feature transformation and fusion strategy was introduced to improve classification effectiveness by addressing high correlation among raw spectral features (Fig. 6). This strategy combines the non-linear dimensionality reduction and feature learning capabilities of a Feedforward Artificial Neural Network (FANN) with a 1024-512-256-32 architecture and class probabilities derived from a Random Forest (RF) classifier. This FANN-RF fusion approach represents a novel contribution not previously explored in radar-based gait analysis literature.
- A comprehensive evaluation was performed using ten diverse Machine Learning (ML) classifiers (PAC, HGBC, CatBoost, LGBM, XGBoost, RC, LDA, RF, MLP, and ETC). All classifiers were rigorously trained and evaluated on the transformed feature set using exhaustive grid search for hyperparameter tuning to ensure optimal and fair comparison (Table 3).
- The proposed FANN-RF fusion approach demonstrated state-of-the-art performance in radar-based gender classification, achieving a peak accuracy of 94.68% and an F1-score of 95% with the Random Forest classifier (Table 4). This outperformed baseline models using only original spectral features (e.g., 88.5% accuracy for RF on original features). The robustness of the approach was further validated through a 5-fold cross-validation score of 0.93 ± 0.01 for the RF model (Table 5).
- This work advances the field by exclusively leveraging UWB radar for contactless gait analysis, distinguishing it from prior studies that relied on vision-based systems or inertial sensors. The integration of enhanced clutter removal, adaptive peak detection tailored for radar signals, and the novel FANN-RF feature fusion strategy together contribute a substantial methodological advancement in improving gender classification efficacy in radar-based human sensing.

2. Literature review

This section reviews the existing literature on gender classification using gait analysis. Studies are grouped thematically based on the technology and methodology employed: vision-based approaches, wearable sensor-based techniques, radar-based systems, and hybrid deep learning methods. A comparative analysis highlights each group's contributions, challenges, and how they inform or contrast with our proposed method using UWB radar.

2.1. Vision-based approaches

Vision-based gait analysis has gained prominence due to its non-invasive nature and compatibility with surveillance systems. Microsoft Kinect and other depth cameras have been extensively used in prior work. For instance, in [25], a statistical model using Kinect-derived 3D joint data achieved a 97.5% accuracy. Similarly, Azhar et al. [26] employed joint coordinates with logistic regression, reaching 98% accuracy.

Some researchers combined deep learning with vision techniques. The study [37] explored CNN-based feature extraction with an SVM classifier, achieving 87.94% accuracy on the CASIA-B dataset. The work in [38] used silhouette-based wavelet features and PCA-C4.5 classifiers to achieve high accuracy on CASIA-B and OU-ISIR datasets (97.9% and 97.5%). Vision methods, while effective, often suffer from limitations in real-world settings due to lighting variation, occlusion, and camera angle dependency.

2.2. Wearable sensor-based approaches

Several studies leverage inertial sensors in smartphones or dedicated wearable devices. For example, Jain and Kanhangad [39] used Histogram of Gradient (HG) features from mobile accelerometers with a bagging classifier to reach 94.44% accuracy. The authors of Nutakki et al. [40] experimented with SVM, decision trees, Naive Bayes (99%), and Random Trees (83%) using mobile sensor data.

Work in [20] evaluated smartphone-based gait patterns using several classifiers (DT, SVM, KNN, LSTM), achieving 94.11%. Khabir et al. [41] explored age and gender classification using inertial sensor data, with SVM reaching 84.76%. However, wearable methods face issues such as user compliance, inconsistent sensor placement, and battery limitations.

2.3. Radar-based systems

Radar offers robust gait sensing in uncontrolled environments and under occlusion. Micro-Doppler radar studies like Ni and Huang [42] used m-D signatures for identifying walking styles, achieving 96.7% accuracy. The work in [43] applied UWB radar with preprocessing and dimensionality reduction, achieving 93.6% accuracy with an MLP classifier.

Radar-based approaches overcome visual occlusion and lighting issues but often require complex signal processing pipelines and are constrained by limited dataset diversity. Our proposed system builds upon this line of research by incorporating a larger, diverse cohort and improved signal fusion and feature extraction, aiming to boost generalizability.

2.4. Hybrid and deep learning approaches

Deep learning approaches often combine spatial and temporal gait features. In [44], a CNN with MFM units handled mislabeled data and achieved 92.7% accuracy. The ASTL framework in [45] introduced attention-aware spatiotemporal learning and reached 97% accuracy. Lau and Chan [46] proposed a hierarchical CNN tree model achieving 99.11% on multi-view gait data.

Additionally, entropy-based methods like GEnEI and AVGEnEI were explored in [47], combined with SVM and KNN (up to 97.3% accuracy). Although effective, many of these models are resource-intensive and often trained on homogeneous datasets, which reduces real-world performance.

2.5. Limitations and motivation for the proposed study

Despite the impressive performance reported in various studies on gait-based gender classification, several important limitations persist across the literature. A common issue is the reliance on data collected in highly controlled environments, such as laboratories or indoor spaces with ideal lighting and minimal distractions. While these conditions ensure data precision, they fail to replicate the complexity of real-world scenarios where factors such as uneven terrain, varying surfaces, crowd density, or occlusion significantly affect gait. As a result, models trained on such data often struggle to generalize well in practical applications.

Another critical limitation lies in the hardware dependency observed in many approaches. Techniques that utilize depth cameras (e.g., Kinect), frequency-modulated radar, or wearable inertial sensors offer precise measurements but are not always feasible for continuous or scalable deployment due to cost, maintenance, or user compliance. For instance, systems requiring users to carry smartphones or wear dedicated sensors assume consistent placement and usage, which is rarely guaranteed outside experimental settings.

Furthermore, the majority of existing datasets used for training and evaluation lack sufficient diversity in terms of gender, age, body types, walking speeds, and environmental conditions. This narrow scope hinders the robustness and inclusiveness of the developed models. Finally, while deep learning methods have achieved high classification accuracy, they often require extensive computational resources and large labeled datasets, posing challenges for real-time implementation and adaptability.

These limitations highlight the need for a more robust and generalizable approach—one that works effectively in unconstrained environments, accommodates varied walking patterns, and requires minimal reliance on specialized or wearable hardware. This study addresses these gaps by utilizing UWB radar technology and an enhanced signal processing pipeline, combined with a diverse participant dataset and a novel feature fusion methodology designed for real-world applicability.

3. Proposed methodology

This section outlines the complete pipeline used for gender classification based on UWB radar gait data. It details the sequential steps, from data collection and signal processing to feature extraction, transformation, and classification. The goal is to present a reproducible methodology that transforms raw radar data into meaningful predictions. The study presented in this manuscript focuses on the task of gender classification by employing gait data obtained using UWB radar technology. The framework of the process is shown in Fig. 1, indicating the sequential progression of steps involved. The first stage involves the collection of raw radar data from people of both genders. Following that, a thorough preprocessing phase is implemented, which includes techniques for refining and cleaning the data. Moreover, the use of feature extraction techniques is implemented, facilitating the extraction of relevant information from the gathered gait data. After the preprocessing and feature extraction stages are finished, the obtained features are subjected to a transformational process. Subsequently, these transformed features are strategically divided into two sets for training and testing purposes. In the next stage, various ML classifiers that are designed. These classifiers are trained using transformed gait features. The classifiers undergo rigorous training to effectively identify complex patterns and inherent traits present in the data, hence facilitating precise gender classification. In the final stage, the trained classifiers undergo a thorough evaluation process using a test set. The assessment procedure employs a variety of metrices, such as accuracy, F1-score, precision, and recall. These metrics offer a thorough evaluation of the classifiers' performance, providing insights into their capacity to reliably determine gender based on the distinct gait patterns exhibited by individuals.

3.1. Data collection

This subsection describes how the raw radar gait data were collected using a UWB radar system. It provides information on the hardware setup, participant demographics, data volume, and ethical considerations, which form the foundation for subsequent processing and analysis. The study used a Time Domain PulsON 410 monostatic radar module (P410) for data collection, as seen in Fig. 2 by the red circular area. The monostatic radar setup used by this module has omnidirectional antennae. The operational requirements of the radar system are in accordance with the criteria set forth by the Federal Communications Commission (FCC). The device generates radio waves within the frequency range of 3.1 GHz to 5.3 GHz, with a central frequency of 4.3 GHz, thereby complying with the restrictions set forth by the FCC [29,31,34,35]. The P410 system has an operational bandwidth of 2.2 GHz. The P410 device meets the requirements outlined for UWB systems [29,31,34,35,48], since it exhibits a fractional bandwidth that surpasses 50%, particularly measuring 51.16%. The system's adherence to the constraints imposed by the FCC highlights its compliance with regulations governing UWB technology [29,31,34,35].

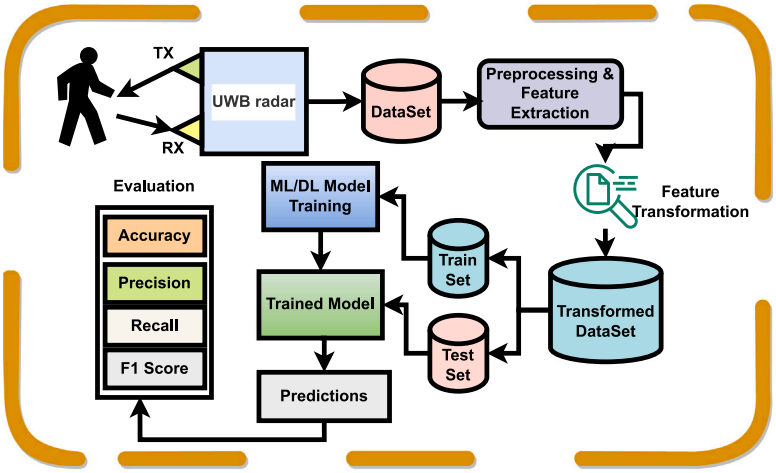

Fig. 1. Proposed methodology diagram.

Fig. 2. Subject moving toward P410 radar mounted on stand and encircled red.

The P410 equipment was carefully configured before to data collection, and this configuration was maintained for both genders throughout the trial as show in Table 1.

Data were collected from both male and female KFUEIT students. The study included a diverse group consisting of 163 participants, with 88 males and 75 females between the ages of 18 and 24. In order to enhance the flexibility and dependability of the study, an extensive set consisting of 1630 data points was obtained, encompassing 10 unique observations for each participant. The study presented in this manuscript was conducted with a strong emphasis on ethical considerations. The study underwent a thorough evaluation by the ethics committee at KFUEIT to assure adherence to ethical norms as defined in the Helsinki Declaration, prior to the commencement of data collection. Informed consent was obtained from all participants, expressing their awareness of the potential risks and benefits connected with their involvement in the trial. The radar equipment was placed at a height of 72 cm on a stand. A Raspberry Pi (RPi) device and a Virtual Network Computing (VNC) viewer have been combined in a seamless manner, thanks to technological developments that improved the effectiveness of the data gathering process and allowed for convenient remote access to the RPi as well as remote control of the radar system. Each participant's interaction with the radar system followed a set

Table 1
Radar configuration for the experiment.

Parameter	Values
Center frequency	4.3 GHz
Frequency range	3.1 GHz to 5.3 GHz
Scan window	5 s
Height	72 cm
Transmit gain	−12.64 dBm
Radar range	9.5 m
Antennas	One Tx and one Rx
Operating temperature	Between 0 °C to 70 °C

protocol. The participants were given explicit instructions to approach the radar system from a fixed distance of 9 m. Participants were asked to maintain a frontal orientation, as depicted in Fig. 2. During the course of this interaction, the process of data recording was carried out for a duration of 5 s for each participant. It is important to note that variables such as walking speed, footwear, and physical conditions were not strictly controlled during data collection to better reflect realistic and unconstrained scenarios. After the data was gathered, it was carefully organized by separating it into directories labeled "Male" and "Female".

3.2. Signal processing and feature extraction

This subsection presents the steps taken to convert raw radar scans into structured data and extract meaningful gait features. It covers the radar data matrix formulation, clutter removal, peak detection, gait cycle segmentation, and feature computation.

3.2.1. Radar data representation

The radar scan gets transformed into a matrix as shown in Figure (a) structure, with a duration of 5 s. Each column of the matrix corresponds to a vector that records the return signal from the radar in the fast time domain. Similar to this, each row in the matrix contains a vector that records the radar's return signal in the slow time domain and is associated with a particular fast time event. The radar's effective indoor scanning range is 9.5 m, yielding a total of 1440 columns. Each column represents a unique distance from the radar. The calculation for determining the distance covered by a singular column is as follows: The total distance covered by the scan, measured in centimeters, is 950 cm. The total number of columns is 1440. Each column covers a distance of 950/1440 = 0.659 cm. Each individual column within the matrix contains a vector of radar return signals that correspond to a specific distance of 0.659 cm from the radar. In order to accurately measure the walking pattern, a designated set of columns, ranging from 200 (≈130 cm) to 860 (≈567 cm) total distance equal to 437 cm, is chosen.

3.2.2. Clutter suppression using pulse canceller

A three-pulse canceller approach given in Eq. (1) is used to improve data quality by lowering clutter interference. This technique attenuates stationary reflections by subtracting delayed pulses, thereby enhancing the visibility of moving targets, such as limbs during gait—while suppressing static background noise. This directly improves the signal-to-clutter ratio and ensures that only dynamic micro-Doppler components relevant to gait are retained.

$$R_{output} = R_i - 2R_{i-1} + R_{i-2} \tag{1}$$

The R_{output} is obtained by subtracting the present radar return signal R_i from twice the preceding radar return signal R_{i-1}, and then adding the radar return signal from two locations earlier R_{i-2}. The purpose of this procedure is to efficiently reduce unnecessary elements and unwanted distortions that are inherent in the original data. The output signal, denoted as R_{output}, demonstrates a finer representation of the radar response, resulting in improved clarity and coherence. The amplified signal is then appropriate for conducting more comprehensive analysis and deriving significant interpretations. The practical application of the equation is shown in Fig. 3, which presents the radar scan before and after implementing the pulse canceller approach. The Fig. 3(b) shows how this mathematical alteration helps to produce a more distinct and visually informative radar signal.

3.2.3. Peak detection for gait cycle identification

After effectively removing extraneous data from the radar dataset, the identification of the gait cycle was achieved by the utilization of peak detection technique. The application of this technique facilitated the identification of noteworthy events occurring during the gait cycle within the radar data. Each identified peak represents an important event that occurred at a notable point in the gait cycle. In order to enhance the process of peak detection, the radar signal was partitioned into two different segments based on columns. A threshold of $0.9e^5$ was established for the first half of the signal. This higher threshold was selected in order to capture the significantly stronger signals closer to the radar. In contrast, the latter part of the signal, which corresponds to higher distances from the radar, had a lower threshold of $0.35e^5$. This modification adjusted for the decrease in signal amplitude caused by increasing distance from the radar. Gait-related signals can be identified by peaks in each column that exceed these set thresholds. The peak detection condition is defined in Eq. (2).

$$P = \left\{ t \,\middle|\, S_c(t) > T_c \wedge S_c(t) > S_c(t-1) \wedge S_c(t) > S_c(t+1) \right\} \tag{2}$$

where $S_c(t)$ is the signal at time t for column c, and T_c is the empirically defined threshold for that region. Peaks are required to be local maxima and spaced by a minimum time interval to ensure detection of distinct gait events. No peak smoothing was applied to preserve fine-grained motion details.

These threshold values were empirically chosen based on iterative testing on a representative dataset. A sensitivity analysis was conducted where thresholds were varied by ±20%, and it was observed that the selected values ($0.9e^5$ and $0.35e^5$) provided the best trade-off between eliminating false positives and retaining genuine gait cycle peaks. This empirical validation supports the robustness and generalizability of the chosen thresholds. Fig. 4 presents the detected peaks within the clutter-removed radar data, serving as a visual representation of the effectiveness of the peak detection procedure.

The gait cycle is a significant temporal segment within the radar signal, which includes the physiological activity associated with walking. The gait process is defined by crucial events, that are identified as peaks in the radar signal. A window of size 111 was used, centered around each detected peak, to accurately capture the gait cycle. The determination of the window size was based on empirical study findings [49] that suggest the average steps length of an individual is around 76.2 cm, that corresponds to approximately ≈111 columns in the radar signal. Although the average step length of 76.2 cm is referenced from [49], which is based on Western population data, this estimate may not precisely reflect the anthropometric characteristics of the Pakistani cohort in this study. To assess its suitability, a visual inspection of radar-derived gait cycles was conducted across representative samples. The observed average step lengths ranged between 73 cm and 77 cm, demonstrating close agreement with the cited value. Therefore, the selected window size of 111 columns (≈76.2 cm) is considered appropriate for capturing the gait cycle in the present dataset and ensures methodological consistency without introducing significant deviation.

Determining the initial and final indices for the window required a detailed method. At the beginning, the window is made precise and limited to the area of the data, so as not to go outside and make mistakes in radar interpretation. To get started, the index of the peak is decreased by half the width of the window. This makes it possible for the window to pick up the radar data, as well as to feature data from before the peak within its set boundary. The strategy helps enclose vital gait information while keeping any extra data taken beyond the

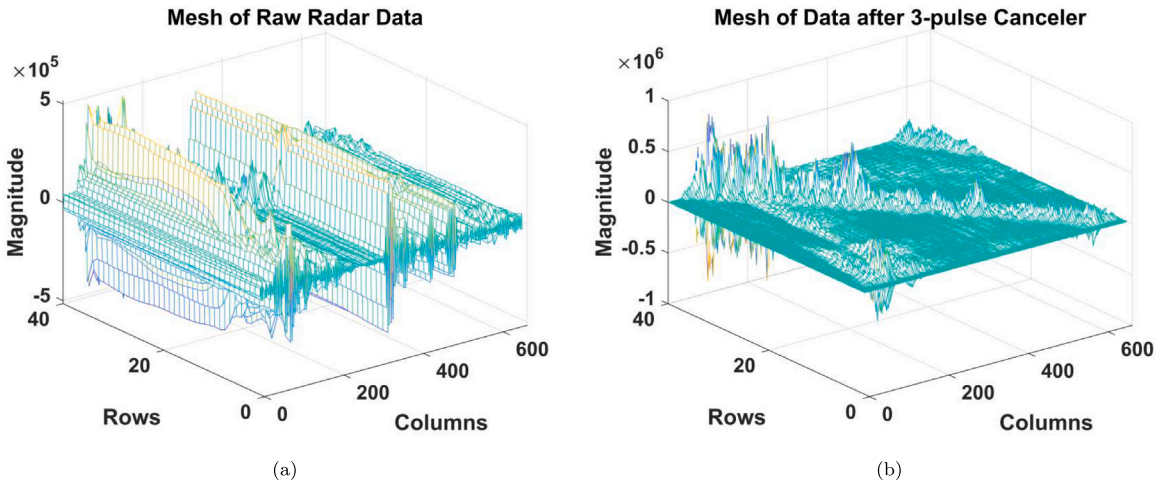

Fig. 3. Illustration of pulse canceler, (a) Radar scan before pulse canceler, and (b) Radar scan after application of pulse canceler.

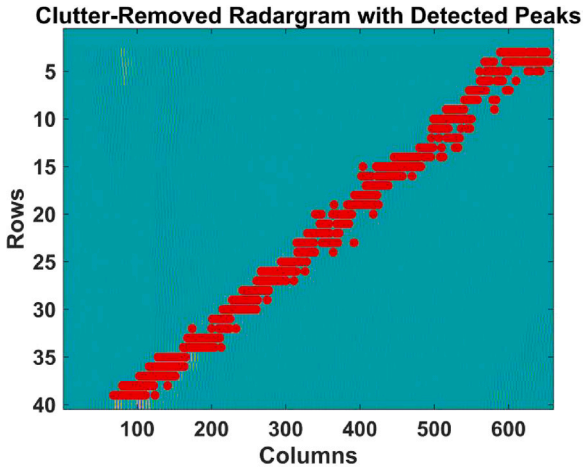

Fig. 4. Radargram with detected peaks.

scanner's range or incidents at the window edge to a minimum. The procedure for ending the index is the same: increase the found peak's index by half the set window's size. Using this method, the radar window tracks what happens after the peak, but makes sure it does not cause the total amount of radar columns to be exceeded. Using the computed indices as the limits properly determines the place where the peak is detected. As a result, the system can pull out the necessary information for study, thus cutting down the risks of errors during data retrieval or indexing. The window is centrally positioned on the peak, and data points that fall within the window are selected to generate the gait cycles, as represented in Fig. 5. This procedure is executed in an iterative manner for each peak that has been discovered in the radar data, leading to the creation of a set of discrete windows that correspond to gait cycles.

3.2.4. Spectral feature extraction

Once the gait cycles were identified, a variety of unique attributes were retrieved from each individual cycle. The most important of these characteristics is the peak amplitude of the gait cycle, which is the highest value prevalent to each cycle. This metric offers useful information on the magnitude of the gait response throughout the gait cycle, facilitating the understanding of physiological processes. To delve deeper into gait activity, the frequency and phase components of each gait cycle were analyzed using the Fast Fourier Transform (FFT) approach. Through the application of FFT analysis, it becomes feasible to detect the distinct frequency components of the gait signal. The use of this analytical approach enables the detection of noteworthy frequency elements that align with gait patterns. Concurrently, the phase information of each gait cycle was acquired by FFT analysis. This phase data is a useful tool for examining the temporal properties of gait function, providing insight into the timing and synchronization of different frequency components within the gait signal. The retrieved features from the gait cycles were subsequently computed as the average across all identified gait cycles. A complete representation of the gait signals collected from the radar scan is given by this thorough averaging.

The key attributes of each radar scan were derived by utilizing the average amplitude, frequency, and phase. These attributes encompass energy entropy (EE), spectral entropy (STE), root-mean-square (RMS), spectral centroid frequency (SCF), spectral kurtosis (SK), spectral skewness (SKNS), spectral roll-off (SR), spectral decrease (SD), spectral flatness (SFLT), spectral contrast (SC), spectral flux (SF), spectral spread (SSP), and spectral slope (SSL). For more information about these features readers are directed to Lalitha et al. [50], Yantorno et al. [51], Siddiqui et al. [52], Tamarit et al. [53], Siddiqui et al. [54], Hosseinzadeh and Krishnan [55], Antoni [56] and Krishna et al. [57]. The selection of 13 spectral features for characterizing radar-derived gait cycles is justified by their proven efficacy in capturing essential frequency-domain characteristics of periodic signals, coupled with their computational efficiency and interpretability. Gait, being an inherently rhythmic and repetitive motion, manifests distinct patterns in the frequency domain, which these features effectively quantify. Attributes such as Spectral Centroid Frequency, Spectral Flux, and Spectral Spread directly reflect the core rhythm and variability of walking. Meanwhile, measures like RMS, Energy Entropy, Spectral Kurtosis, and Spectral Flatness provide valuable insights into the overall signal power, energy distribution, and the consistency of the spectral shape, all of which are critical for distinguishing different gait patterns. While wavelet-based or hybrid time-frequency features excel at localizing non-stationary events in both time and frequency, our chosen spectral features offer a robust and computationally lean approach to characterize the quasi-periodic nature of gait signals within the defined analysis windows. This balance of detailed frequency information and practical computational demands makes them a suitable and effective choice for this radar-based gait analysis. Prior studies have demonstrated the reliability of similar features in related tasks. For instance, Saleem et al. [43] employed spectral features for gender classification using UWB radar. In another study [42], micro-Doppler signatures analyzed through frequency-based features for gender classification. Furthermore, accelerometer-based studies such as Khabir et al. [41] and Sabir et al. [20] also relied on spectral metrics to successfully

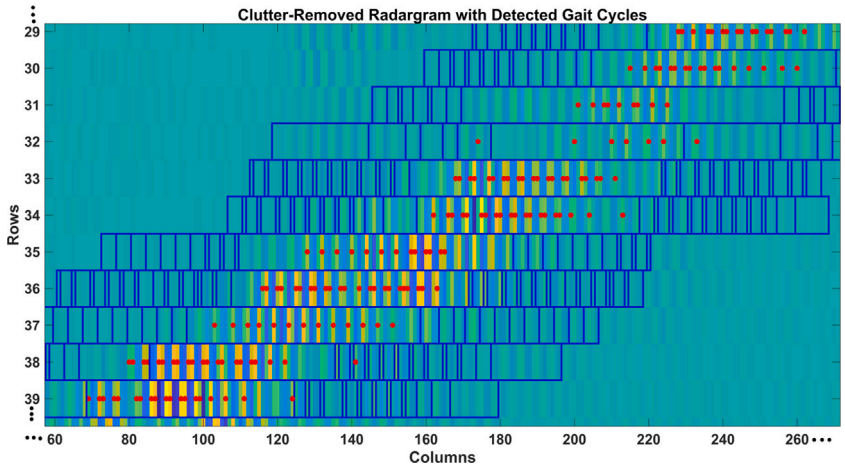

Fig. 5. Clutter removed radargram with detected gait cycles.

distinguish gender-related gait patterns. While wavelet-based or hybrid time-frequency features may offer enhanced resolution, the selected spectral features provide a balanced trade-off between discriminative power and computational efficiency. Within the framework of classification, a distinct label was assigned to each set of extracted features, serving as an indicator of the class to which the relevant radar scan belongs. Within this particular framework, the Male category was denoted by the numerical label 0, whilst the Female category was denoted by the numerical label 1. In order to enable subsequent analysis, the feature sets and their accompanying labels were carefully documented and saved in a CSV file. The implementation of this approach guarantees the presence of well-arranged and well labeled data that can be utilized in following phases of analysis and machine learning.

3.3. Feature transformation

The objective of this subsection is to enhance the quality and interpretability of the extracted features through dimensionality reduction. Exploring a dataset consisting of spectral features necessitates visualizing the interrelationships between these features; however, it is challenging to directly visualize a high-dimensional dataset due to human perceptual limitations. However, there are effective solutions available to address this difficulty. These strategies involve the use of dimensionality reduction techniques and other visualization approaches to extract significant insights from complex datasets. A frequently employed strategy involves the utilization of dimensionality reduction techniques such as Principal Component Analysis (PCA) or t-distributed Stochastic Neighbor Embedding (t-SNE) to convert the data into a lower-dimensional space, often two-dimensional or three-dimensional, while retaining important structural characteristics. In this study, PCA is used to extract the principal components of the dataset. These components are obtained as linear combinations of the original spectral features. The initial five principal components hold particular significance since they effectively reflect the most prominent patterns of variance present within the dataset. A pair plot illustrated in Fig. 6, a visualization tool that enables the examination of relationships between pairs of dimensions, is built using these principal components.

The pair plot shown in Fig. 6 reveals that the original spectral features exhibit substantial correlation, which can hinder the ability of ML algorithms to learn meaningful discriminative patterns. To address this issue, a novel feature transformation and integration approach was introduced that enhances the separability of classes by creating a more discriminative and less redundant feature space. This is achieved by combining the non-linear transformation capabilities of a Feedforward Artificial Neural Network (FANN) with the probabilistic outputs of a Random Forest (RF) classifier. This fusion leverages the complementary strengths of both models—FANN as a deep feature extractor and RF as a robust ensemble learner.

In our proposed methodology, each sample's original spectral feature vector $\mathbf{x} \in \mathbb{R}^D$ is first passed through a multi-layer FANN. The architecture comprises four hidden layers with 1024, 512, 256, and 32 neurons respectively, each followed by a ReLU activation function as given in 2. The transformation can be expressed as: $\mathbf{h}_0 = \mathbf{x}$, followed by $\mathbf{h}_k = \text{ReLU}(W_k\mathbf{h}_{k-1} + \mathbf{b}_k)$ for $k = 1, \ldots, L$, where $L = 4$ is the number of hidden layers. The output from the final layer $\mathbf{h}_L$ serves as the transformed feature vector $\mathbf{f}_{FANN} \in \mathbb{R}^{D_{FANN}}$. This process is repeated for all N samples to yield the transformed feature matrix $F_{FANN} \in \mathbb{R}^{N\times D_{FANN}}$.

Simultaneously, a RF classifier is trained using the original 13 spectral features. This model, configured with `max_depth=10`, `n_estimators=10`, and `random_state=0`, outputs a class probability vector $\mathbf{p}_{RF}(\mathbf{x}) \in \mathbb{R}^C$ for each input $\mathbf{x}$, where C denotes the number of classes. These probability vectors represent the RF's confidence for each class, based on the aggregated votes across its ensemble of trees. For all samples, the corresponding class probability matrix $P_{RF} \in \mathbb{R}^{N\times C}$ is obtained.

The final feature representation is created by horizontally concatenating the FANN-transformed features with the RF class probabilities. For a single sample, this results in a fused feature vector $\mathbf{f}_{fused} = [\mathbf{f}_{FANN} \quad \mathbf{p}_{RF}(\mathbf{x})] \in \mathbb{R}^{D_{FANN}+C}$, and collectively across all samples, the complete fused feature matrix $F_{fused} = [F_{FANN} \quad P_{RF}] \in \mathbb{R}^{N\times(D_{FANN}+C)}$ is formed. The distribution of the fused features is visualized in Fig. 7.

This transformation-fusion pipeline brings together distinct yet complementary sources of information. The FANN serves to capture complex, non-linear relationships between the original spectral features and class labels, effectively acting as a non-linear dimensionality reduction tool. The RF's class probability outputs, on the other hand, introduce a decision-level perspective that encodes the classifier's uncertainty and learned boundaries in a structured way. The combined representation allows downstream classifiers to benefit from both abstract feature embeddings and ensemble-based confidence scores, improving the overall robustness and generalization ability of the model. Importantly, this fusion does not introduce any data leakage or bias, as the RF is trained independently on raw spectral inputs and contributes only probabilistic outputs rather than labels or ground truth information.

The specific configuration of the FANN was determined through extensive empirical tuning. Architectures with varying numbers of layers and neurons were tested, with performance evaluated based on classification accuracy, training stability, and computational efficiency. The selected 1024-512-256-32 layout offered the best balance between expressive power and model simplicity. The gradual reduction in layer size encourages hierarchical abstraction and enforces a bottleneck

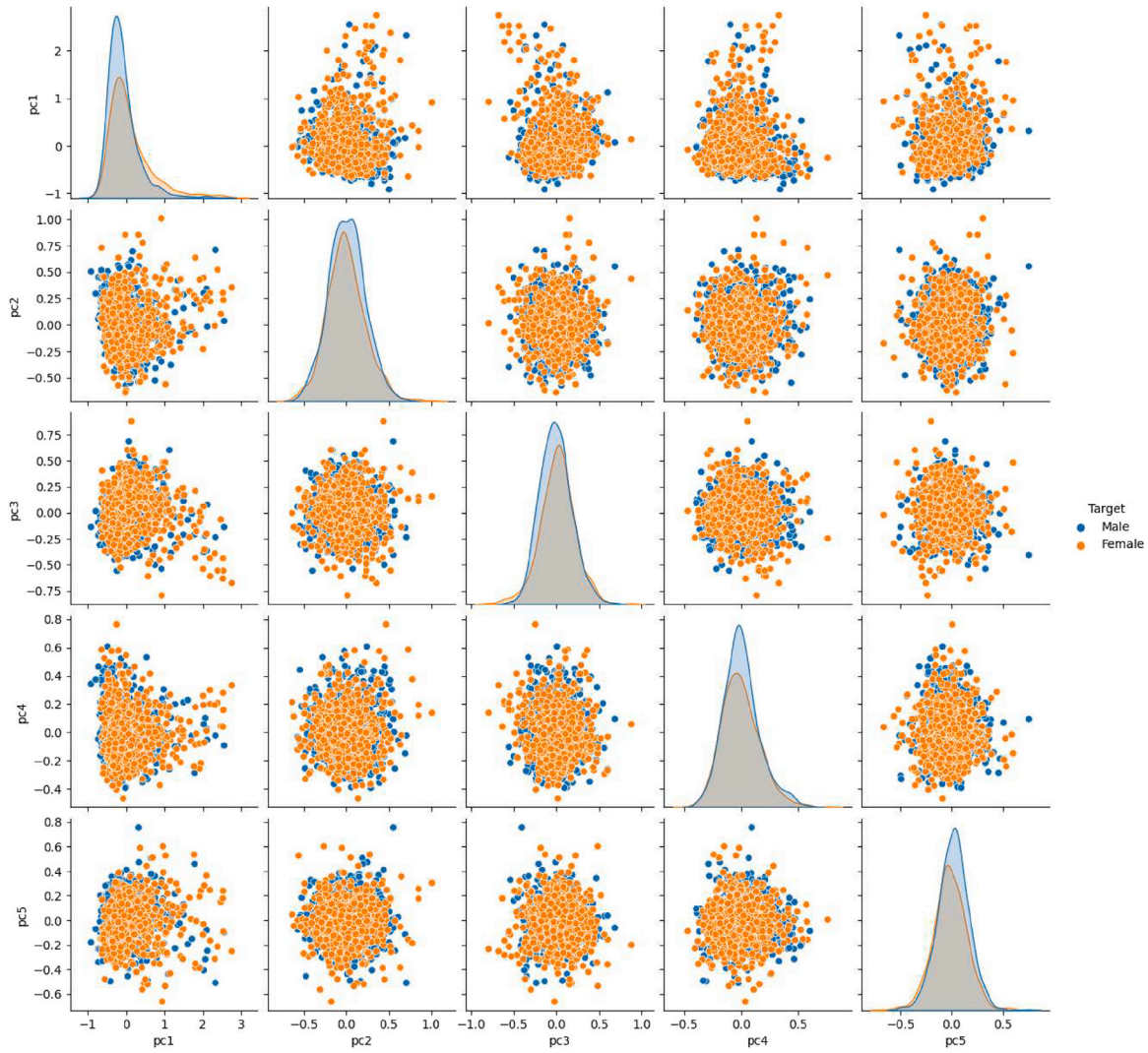

Fig. 6. Pair plot of the first five principal components of the spectral feature dataset.

Table 2
Architecture of the feedforward artificial neural network.

Layer	Activation function	Neurons
Input	None	X
Hidden	ReLU	1024
Hidden	ReLU	512
Hidden	ReLU	256
Output	ReLU	32

effect that helps in filtering out redundant information. FANN was selected over autoencoders and other manifold learning techniques due to its suitability for supervised feature learning. Unlike autoencoders, which primarily aim to reconstruct input data, FANN learns representations optimized for classification. Its feedforward structure, when properly tuned, offers effective non-linear transformations with lower complexity, making it a practical choice for this task.

The pair plot of the first five principal components is depicted in Fig. 8, showcasing the altered feature set. The presented visualization provides compelling observations, unveiling a significant alteration in the attributes of the data following its transformation. Significantly, in comparison to their initial condition, the features currently demonstrate a noticeable level of distinctiveness, suggesting a decrease in the degree of strong correlation. This transformation-driven improvement has the potential to significantly impact subsequent analyzes and ML models, enabling the extraction of more meaningful and distinguishable data patterns.

3.3.1. Numerical example of FANN-RF feature fusion process

To clarify the functionality of the proposed FANN-RF framework, we present a step-by-step numerical example using a simplified gait feature vector. Suppose a preprocessed gait sample extracted from the spectral domain is represented by the following feature vector:

$$\mathbf{x} = [0.12, 0.45, 0.30, 0.58, 0.21]$$

This low-dimensional feature vector is used here for illustrative purposes; in practice, the actual feature space contains significantly more dimensions.

Step 1: FANN feature transformation. The feature vector $\mathbf{x}$ is passed through a trained Feedforward Artificial Neural Network (FANN). Suppose the FANN has one hidden layer with the following weights and biases:

- Hidden layer weights (W_1):

$$\begin{bmatrix} 0.1 & -0.2 & 0.3 & 0.5 & -0.1 \\ -0.4 & 0.2 & 0.1 & -0.3 & 0.4 \end{bmatrix}$$

- Hidden layer biases (b_1): $[0.05, -0.03]$

	F0	F1	F2	F3	F4	F5	F6	F7	F8	F9	...	F24	F25	F26	F27	F28	F29	F30	F31	F32	F33
0	0.813423	0.186577	0.067051	0.0	0.000000	0.000000	0.172010	0.0	0.279345	0.131745	...	0.0	0.000000	0.000000	0.0	0.234449	0.0	0.082320	0.000000	0.386723	0.109084
1	0.891511	0.108489	0.623423	0.0	0.000000	0.000000	0.772167	0.0	0.484979	0.190049	...	0.0	0.000000	0.000000	0.0	0.648639	0.0	0.000000	0.000000	0.951722	0.000000
2	0.732984	0.267016	0.000000	0.0	0.000000	0.000000	0.000000	0.0	0.049611	0.052569	...	0.0	0.000000	0.036128	0.0	0.142809	0.0	0.109350	0.000000	0.052523	0.057281
3	0.690150	0.309850	0.120711	0.0	0.000000	0.000000	0.208999	0.0	0.277553	0.137737	...	0.0	0.000000	0.000000	0.0	0.271721	0.0	0.101749	0.000000	0.406797	0.069892
4	0.778375	0.221625	0.050915	0.0	0.000000	0.000000	0.100696	0.0	0.184207	0.115869	...	0.0	0.000000	0.000000	0.0	0.178937	0.0	0.106411	0.000000	0.276520	0.096852
...	...	...	...	...	...	...	...	...	...	...	...	...	...	...	...	...	...	...	...	...	...
1625	0.106359	0.893641	0.000000	0.0	0.020837	0.000000	0.000000	0.0	0.042003	0.072250	...	0.0	0.007543	0.000000	0.0	0.134575	0.0	0.124928	0.041898	0.037549	0.069387
1626	0.146393	0.853607	0.064239	0.0	0.000000	0.000000	0.000000	0.0	0.067257	0.020147	...	0.0	0.011468	0.021183	0.0	0.086636	0.0	0.065632	0.009783	0.012902	0.064555
1627	0.129824	0.870176	0.026418	0.0	0.000000	0.021542	0.000000	0.0	0.061807	0.033069	...	0.0	0.000000	0.104963	0.0	0.123824	0.0	0.067471	0.000000	0.000000	0.028841
1628	0.146393	0.853607	0.064239	0.0	0.000000	0.000000	0.000000	0.0	0.067257	0.020147	...	0.0	0.011468	0.021183	0.0	0.086636	0.0	0.065632	0.009783	0.012902	0.064555
1629	0.129824	0.870176	0.026418	0.0	0.000000	0.021542	0.000000	0.0	0.061807	0.033069	...	0.0	0.000000	0.104963	0.0	0.123824	0.0	0.067471	0.000000	0.000000	0.028841

1630 rows × 34 columns

Fig. 7. Transformed feature set.

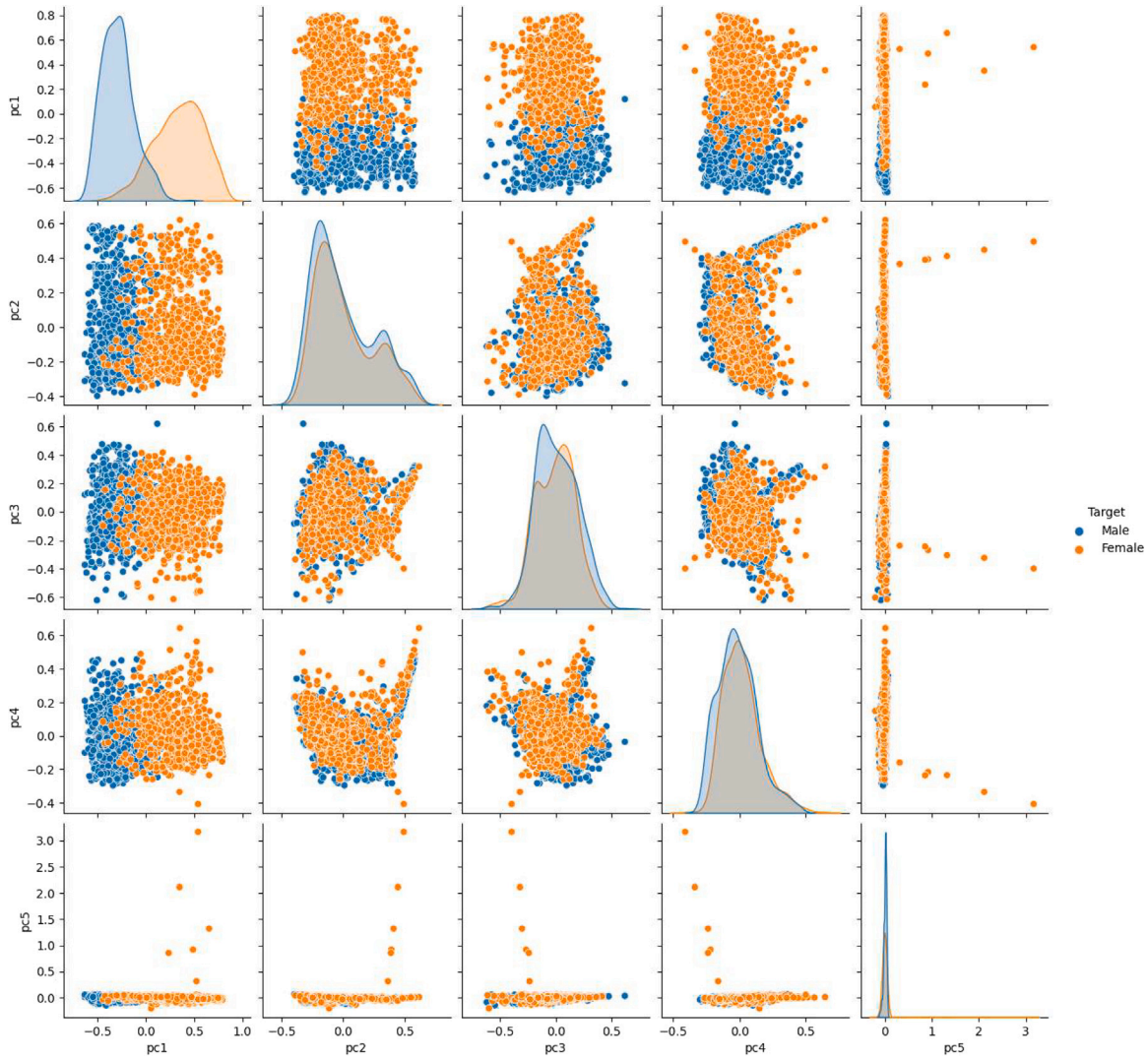

Fig. 8. Pair plot of the first five principal components of the transformed features dataset.

The activation function used is ReLU. The output of the hidden layer is:

$$\mathbf{h} = \mathrm{ReLU}(W_1 \cdot \mathbf{x} + b_1) = \mathrm{ReLU}$$

$$\times \left(\begin{bmatrix} 0.1 & -0.2 & 0.3 & 0.5 & -0.1 \\ -0.4 & 0.2 & 0.1 & -0.3 & 0.4 \end{bmatrix} \cdot \begin{bmatrix} 0.12 \\ 0.45 \\ 0.30 \\ 0.58 \\ 0.21 \end{bmatrix} + \begin{bmatrix} 0.05 \\ -0.03 \end{bmatrix} \right)$$

$$= \mathrm{ReLU}\left(\begin{bmatrix} 0.285 \\ -0.188 \end{bmatrix} \right) = \begin{bmatrix} 0.285 \\ 0 \end{bmatrix}$$

This transformed feature vector $\mathbf{h} = [0.285, 0]$ is the high-level representation learned by the FANN.

Step 2: Random forest classification. The transformed vector is then fed into a trained Random Forest classifier. Suppose the RF classifier outputs the following class probabilities:

$$P(\text{Male}) = 0.78, \quad P(\text{Female}) = 0.22$$

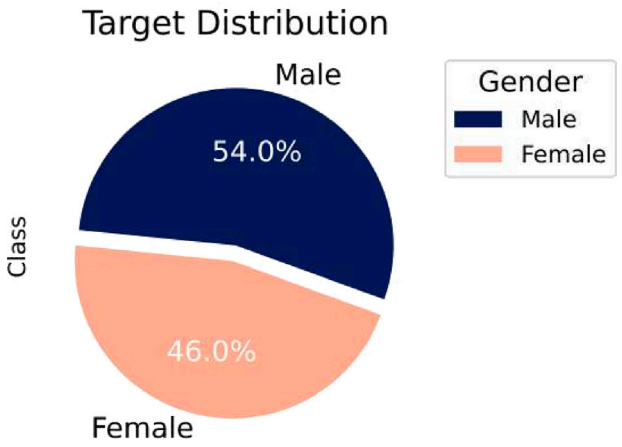

Fig. 9. Distribution of the labels in the dataset.

Based on this result, the classifier assigns the "Male" label to the input instance with high confidence.

This example illustrates how the FANN network extracts abstract nonlinear patterns from the spectral features, reducing redundancy and improving separability. The RF classifier then utilizes its ensemble decision structure to robustly classify the instance, ultimately enhancing the overall system performance.

4. Results and discussions

This section presents the experimental outcomes of the proposed FANN-RF approach for gender classification using gait data captured via UWB radar. It includes dataset details, baseline and enhanced classification performance, cross-validation results, and a comparison with existing studies. Additionally, the implications of the findings, limitations, and directions for future work are discussed in depth. The dataset comprises a total of 1630 instances, with 880 instances corresponding to males and 750 instances corresponding to females. The distribution of the dataset, shown by a pie chart in Fig. 9, reveals that the male class accounts for 54% of the instances, demonstrating a comparatively greater representation. Conversely, the female class makes up 46% of the occurrences. The distribution of gender within the dataset is emphasized, serving as a crucial basis for later analysis and classification endeavors. The dataset was divided into two sets using a 70–30 split. Specifically, 70% of the instances were allocated for training purposes, while the remaining 30% were reserved for testing. The process of dividing the data into subsets guarantees that a significant proportion of the data is allocated for training the classification model. This allocation allows the model to acquire knowledge and make generalizations based on the patterns found in the gait attributes. The testing subset that is reserved acts as a separate set for evaluation, enabling the assessment of the model's performance on data that it has not been exposed to previously. This allows for a reliable measure of the model's ability to classify accurately.

A comprehensive evaluation of the classification task was conducted using a variety of different machine learning classifiers. The classifiers consisted of the passive-aggressive classifier (PAC), Hist Gradient Boosting Classifier (HGBC), CatBoost, LGBM, XGBoost, Ridge classifier (RC), Linear Discriminant Analysis (LDA), RF, MLP classifier, and ExtraTrees classifier (ETC). To improve the performance of these models, an exhaustive grid search was performed to precisely tweak the hyperparameters for each classifier. As a result of this procedure, the ideal hyperparameters were identified and are listed in Table 3. The primary objective of this rigorous approach for hyperparameter tuning is to optimize the performance of the classifiers. This optimization process ultimately enables precise gender classification by leveraging the retrieved gait features.

Table 3
Hyperparameters of the classifiers.

Classifier	Parameters
PAC	`max_iter = 100, random_state = 0`
HGBC	`max_iter = 100, random_state = 0`
CatBoost	`iterations = 200, depth = 10, learning_rate = 0.1, loss_function = 'Logloss'`
LGBM	Default
XGBoost	`n_estimators = 1000, learning_rate = 0.1, max_depth = 6, objective = 'binary:logistic'`
RC	`alpha = 1.0`
LDA	Default
RF	`random_state = 142, max_depth = 150, n_estimators = 150`
MLP	`random_state = 142, activation = 'tanh', max_iter = 200`
ETC	`n_estimators = 100, max_depth = 200, random_state = 0`

Table 4
Test accuracy (%) of classifiers on original spectral features (baseline).

Classifier	Test accuracy (%)
PAC	54.29
HGBC	62.27
CatBoost	62.27
LGBM	61.04
XGBoost	63.80
RC	61.04
LDA	61.35
RF	59.20
MLP	62.88
ETC	58.28

4.1. Baseline performance on original features

To establish a reference point for evaluating the effectiveness of the proposed FANN-RF fusion strategy, an experiment was conducted using ten standard ML classifiers trained directly on the original spectral features as shown in Table 4. The results reveal relatively modest classification performance, with the highest test accuracy of 63.80% achieved by XGBoost, followed by MLP at 62.88% and CatBoost and HGBC both at 62.27%. In contrast, the RF classifier achieved only 59.20% accuracy on the raw features. These results suggest that the original spectral features, though informative, contain redundancies and nonlinear correlations that are not easily separable by standard classifiers. This motivates the need for advanced feature transformation. The proposed FANN-RF feature fusion strategy addresses this by leveraging the nonlinear feature learning capacity of a FANN alongside the probabilistic decision boundaries derived from RF classification probabilities.

4.2. Performance on FANN-RF fusion features

The evaluation of different ML classifiers on a dataset that involves gender classification using gait data yields valuable insights regarding the effectiveness of each model. The evaluation criteria employed, namely Accuracy, Precision, Recall, and F1-score, provide an in-depth understanding of the classifiers' capabilities. The classification metrices of different classifiers in Table 5.

The results presented in Table 5 and visualized in Fig. 10 emphasized a number of exceptional performers. The CatBoost algorithm exhibited remarkable accuracy, with a score of 94.27%. Additionally, it achieved precision, recall, and F1-score values of 94% that were well-aligned. The RF exhibited notable consistency and accuracy, achieving

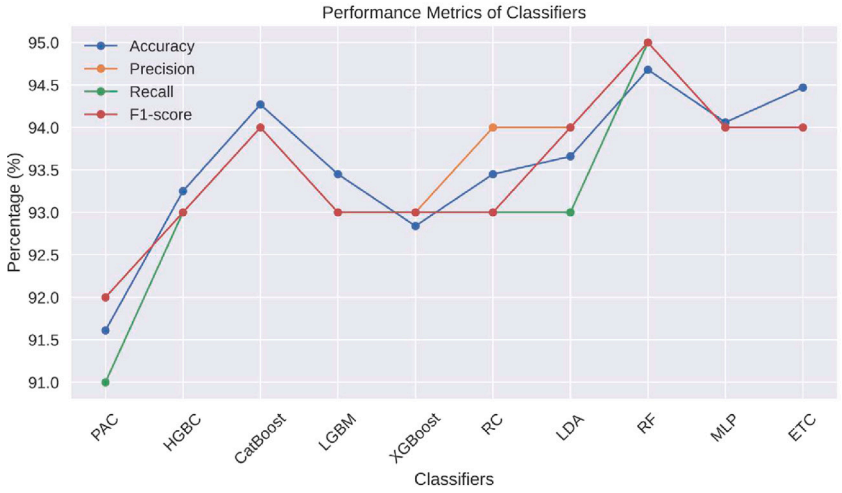

Fig. 10. Visualization of performance metrics of classifiers.

Table 5
Performance metrics of classifiers.

Classifier	Accuracy (%)	Precision (%)	Recall (%)	F1-score (%)
PAC	91.61	92	91	92
HGBC	93.25	93	93	93
CatBoost	94.27	94	94	94
LGBM	93.45	93	93	93
XGBoost	92.84	93	93	93
RC	93.45	94	93	93
LDA	93.66	94	93	94
RF	94.68	95	95	95
MLP	94.06	94	94	94
ETC	94.47	94	94	94

Table 6
Cross validation results of the classifiers.

Classifier	Cross validation score & Standard deviation
PAC	0.90 ± 0.04
HGBC	0.92 ± 0.02
CatBoost	0.92 ± 0.02
LGBM	0.92 ± 0.01
XGBoost	0.92 ± 0.02
RC	0.92 ± 0.02
LDA	0.92 ± 0.02
RF	0.93 ± 0.01
MLP	0.93 ± 0.01
ETC	0.92 ± 0.02

a performance of 94.68%. Additionally, it demonstrated good precision, recall, and F1-score, all of which were at 95%. In a similar vein, the ETC algorithm demonstrated strong predictive skills, achieving an accuracy rate of 94. 47% with corresponding precision, recall, and F1 scores of 94%.

4.2.1. Kfold cross validation

The researchers performed K-fold cross-validation in order to evaluate the reliability and consistency of the classifiers. The validation method utilized a total of five folds. Table 6 summarizes the validation results. Furthermore, Fig. 11 presents a visual depiction of the results. The bar chart in the figure represents the average accuracy of the classifiers, while the error bars indicate the standard deviations associated with these accuracies.

The results presented in Table 6 and visualize in Fig. 11 that PAC shows a consistent cross-validation score of 0.90 ± 0.04, indicating its effectiveness in the task of gender classification. The HGBC, CatBoost, LGBM, XGBoost, RC, ETC, and LDA consistently shows good performance, as indicated by their cross-validation scores of 0.92 ± 0.02. These values highlight the models' ability to achieve a balanced precision and recall. Significantly, the RF and MLP models demonstrated exceptional performance, attaining a cross-validation score of 0.93 ± 0.01. The classifiers exhibited remarkable consistency, successfully recognizing subtle patterns associated to gender.

From the classification results in Table 5 and the validation scores in Table 6, the Random Forest (RF) classifier demonstrates the highest accuracy (94.68%) and strong precision, recall, and F1-score values (all at 95%). Additionally, it achieved the highest cross-validation score (0.93 ± 0.01), indicating both effectiveness and consistency. Among the evaluated classifiers, Random RF achieved the highest performance. This can be attributed to its ensemble-based structure, which combines multiple decision trees to reduce overfitting and handle high-dimensional, nonlinear feature spaces effectively. The FANN-transformed features benefit from RF's ability to model complex interactions without requiring intensive parameter tuning. In contrast, CatBoost and MLP also demonstrated strong results but performed slightly lower than RF. CatBoost, while powerful, is more sensitive to fine-tuning of categorical feature handling and hyperparameters. MLP, being a neural network, may require more extensive training data or optimization to reach peak generalization. The consistent yet marginal differences across models suggest the robustness of the extracted features and confirm the reliability of the proposed pipeline.

4.3. Comparison with existing studies

This section compares the proposed study with previous research that employed various gait-based approaches to gender classification. Table 7 summarizes radar technology (if applicable), number of subjects, classification method, and accuracy achieved. Kim et al. [42] employed frequency-modulated radar with micro-Doppler signatures and achieved high accuracy (96.7%) but only with 20 subjects, limiting generalizability. Similarly, Saleem et al. [43] used the UWB radar and achieved 93. 6% precision with 181 subjects. The proposed study also uses UWB radar, but achieves a slightly better performance of 94.68% using 163 participants, utilizing robust spectral feature extraction and feature fusion techniques.

Several vision- and sensor-based studies have also demonstrated high accuracies. For instance, the study in [25] used Microsoft Kinect and achieved 97.5% accuracy through a statistical model. Likewise, Azhar et al. [26] combined Kinect-based joint features with logistic regression, reaching 98.0%. These methods, while highly accurate, are limited by the requirement of line-of-sight and sensitivity to occlusions.

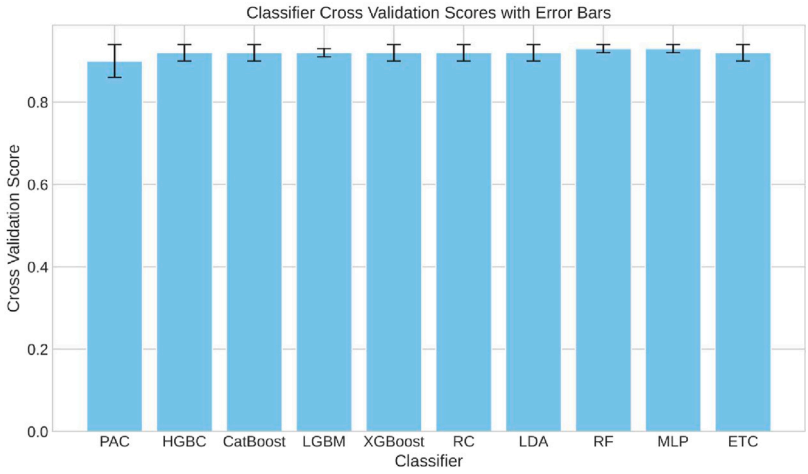

Fig. 11. Visualization of cross validation results of the classifiers with error bars.

Table 7
Comparison with existing gait-based gender classification studies.

Study	Modality/Sensor	No. of subjects	Accuracy
Kim et al. [42]	FMCW Radar	20	96.7%
Saleem et al. [43]	UWB Radar	181	93.6%
Azhar et al. [25]	Kinect + Statistical Model	Not specified	97.5%
Azhar et al. [26]	Kinect + Logistic Regression	Not specified	98.0%
Jain and Kanhangad [39]	Smartphone Sensors + Bagging	Not specified	94.44%
Sabir et al. [20]	Smartphone Sensors + SVM/RNN-LSTM	Not specified	94.11%
Liu et al. [37]	CNN + SVM (CASIA-B)	Not specified	87.94%
Mawlood and Sabir [47]	GEI + Entropy + SVM	Not specified	97.3%
Proposed study	UWB Radar + Spectral Feature Fusion	163	**94.68%**

Smartphone-based methods such as in [20,39] extracted accelerometer and gyroscope features to classify gender, achieving 94.44% and 94.11% accuracy respectively. These methods are promising due to their portability but often lack consistency in unconstrained environments. Hybrid methods, such as CNN+SVM in [37], achieved 87.94% using CASIA-B data, while Mawlood and Sabir [47] introduced entropy-based gait features and reached up to 97.3% using SVM. Despite high performance, these models typically rely on controlled datasets and are not tested in real-time scenarios.

The proposed study strikes a balance between accuracy, real-world feasibility, and dataset diversity. It uses UWB radar, a modality less affected by lighting, occlusion, or clothing variation and integrates signal processing with learning-based feature fusion to ensure robust gender classification.

The proposed approach demonstrates competitive performance compared to both vision-based and sensor-based methods. Its reliance on UWB radar enhances robustness to environmental factors, and its integration of advanced signal processing and machine learning makes it well-suited for real-world applications.

4.4. Discussion

The results presented in this study demonstrate the superior effectiveness of the proposed FANN-RF fusion approach for gender classification based on gait using UWB radar. The baseline evaluation on original spectral features (Table 4) showed that even after careful hyperparameter tuning, conventional classifiers achieved relatively modest accuracy—maximally 63.80% by XGBoost. This indicates that the raw features are not sufficiently discriminative due to underlying nonlinearity, noise, and redundancy. In contrast, the application of the FANN-RF pipeline led to a significant performance boost, with Random Forest achieving a test accuracy of 94.68%, along with balanced precision, recall, and F1-scores of 95%. The consistent improvements across all classifiers when using FANN-RF features (Table 5) and their stable cross-validation performance (Table 6) confirm the effectiveness and robustness of the proposed feature transformation strategy.

The advantages of the FANN-RF fusion approach stem from its dual strengths, FANN serves as a nonlinear feature learner, extracting high-level discriminative representations from spectral gait data, and RF uses its ensemble structure to capture complex decision boundaries without overfitting, making it well-suited for high-dimensional transformed features. This combination allows for effective exploitation of both spectral and structural characteristics of gait signals, which are difficult to separate using standard classifiers on raw features.

However, there are several limitations that must be acknowledged. First, while the dataset size (163 subjects, 1630 samples) is reasonable, the generalizability to more diverse populations e.g., varying age groups, body types, walking conditions, or cultural gait differences has not been explored. Second, the study uses only spectral features extracted from the range-Doppler domain, which might overlook other spatial–temporal cues useful for classification. Third, although FANN-RF performs well, it introduces an additional processing layer that might be computationally heavier than simpler classifiers in real-time applications.

Future work will focus on expanding the dataset to include more diverse subjects (age, gait types, walking conditions) to improve real-world generalizability. A feature ablation study will be conducted to evaluate alternative feature types (e.g., wavelet or hybrid time-frequency features) for enhanced performance. To improve interpretability, Explainable AI (XAI) methods like SHAP and LIME will be integrated, enabling insights into how FANN-transformed features relate to gait traits such as cadence or stride symmetry. For reference, similar approaches have been applied in biosignal analysis by Mowla et al. [58]. Additionally, future work will incorporate multimodal features and adapt the framework for real-time use on embedded systems for applications in healthcare and surveillance.

While the primary focus of this study was on improving classification accuracy for gender identification using gait features, the aspect of

security and resistance to adversarial attacks remains an important consideration for real-world deployment. Radar-based biometric systems, including gait recognition, can be susceptible to spoofing, adversarial perturbations, or data injection attacks, especially in surveillance or healthcare applications. Although this study does not include a dedicated security analysis, future work will explore the robustness of the proposed FANN-RF framework under adversarial conditions. Techniques such as adversarial training, noise resilience testing, and signal perturbation analysis will be considered to ensure the system maintains integrity and reliability under potential attack scenarios. Addressing these concerns is vital for ensuring trust and safety in privacy-sensitive environments.

5. Conclusion

The classification of gender is an essential aspect within various domains, such as security and healthcare. Biometric techniques, which include facial and voice recognition, activity analysis, and gait recognition, have been utilized for the purpose of gender classification. However, these methodologies encounter ongoing challenges such as obstacles caused by body parts, the need for extensive computational resources, and errors in recognition, ultimately affecting their effectiveness and accuracy. To overcome these issues this study explored the field of gender classification by utilizing gait data obtained through the use of Ultra-Wideband radar technology in an innovative way. The initial phase of the investigation involved the thorough collecting of data from an extensive population of 163 people. The raw radar data was subjected to a number of preprocessing procedures, including clutter reduction and peak recognition, in order to extract the relevant information related to the gait cycle. The gait cycle data was used to retrive spectral features. The spectral features that were extracted a transformative procedure, utilizing both Feed Forward Neural Networks and Random Forests, in order to augment their ability to differentiate between different classes. Moreover, the resilience of the system was demonstrated by its strong cross-validation scores of 0.93. Future research will focus on deploying the models in practical, real-world settings where environmental and demographic variations are more pronounced. This includes investigating the robustness of the approach across diverse populations by examining cross-cultural differences in gait, age-related gait variations, and the impact of different clothing types, which may subtly affect radar signatures. Additionally, assessing performance on data from physically disabled individuals will be important to ensure broader applicability. Expanding the dataset to include a larger and more representative sample is essential to improve model generalization and fairness. Moreover, exploring advanced deep learning architectures, such as convolutional neural networks and transformer-based models tailored for time-series radar data, could further enhance classification accuracy and adaptability in dynamic environments

CRediT authorship contribution statement

Adil Ali Saleem: Writing – original draft, Visualization, Validation, Software, Methodology, Investigation, Data curation, Conceptualization. **Hafeez Ur Rehman Siddiqui:** Writing – review & editing, Writing – original draft, Visualization, Methodology, Conceptualization. **Muhammad Amjad Raza:** Visualization, Validation, Software, Methodology. **Sandra Dudley:** Writing – review & editing, Supervision, Project administration. **Julio César Martínez Espinosa:** Project administration, Investigation, Funding acquisition. **Luis Alonso Dzul López:** Project administration, Investigation, Funding acquisition. **Isabel de la Torre Díez:** Writing – review & editing, Supervision, Funding acquisition.

Institutional review board statement

The study was conducted in accordance with the Declaration of Helsinki and approved by the Institutional Review Board (or Ethics Committee) of KFUEIT.

Informed consent statement

Informed consent was obtained from all subjects involved in the study.

Funding

The authors declare that they received no funding for this research study.

Declaration of competing interest

The authors declare that they have no known competing financial interests or personal relationships that could have appeared to influence the work reported in this paper.

Data availability

Data will be made available on request.

References

[1] Abouelenien M, Pérez-Rosas V, Mihalcea R, Burzo M. Multimodal gender detection. In: Proceedings of the 19th ACM international conference on multimodal interaction. 2017, p. 302–11.
[2] Dantcheva A, Elia P, Ross A. What else does your biometric data reveal? A survey on soft biometrics. IEEE Trans Inf Forensics Secur 2015;11(3):441–67.
[3] Seneviratne S, Seneviratne A, Mohapatra P, Mahanti A. Your installed apps reveal your gender and more!. ACM SIGMOBILE Mob Comput Commun Rev 2015;18(3):55–61.
[4] Topaloglu M, Ekmekci S. Gender detection and identifying one's handwriting with handwriting analysis. Expert Syst Appl 2017;79:236–43.
[5] Duong D, Tan H, Pham S. Customer gender prediction based on E-commerce data. In: 2016 eighth international conference on knowledge and systems engineering. KSE, IEEE; 2016, p. 91–5.
[6] Zhang J, Du K, Cheng R, Wei Z, Qin C, You H, Hu S. Reliable gender prediction based on users' video viewing behavior. In: 2016 IEEE 16th international conference on data mining. ICDM, IEEE; 2016, p. 649–58.
[7] You Q, Bhatia S, Sun T, Luo J. The eyes of the beholder: Gender prediction using images posted in online social networks. In: 2014 IEEE international conference on data mining workshop. IEEE; 2014, p. 1026–30.
[8] Deng J, Guo J, Xue N, Zafeiriou S. Arcface: Additive angular margin loss for deep face recognition. In: Proceedings of the IEEE/CVF conference on computer vision and pattern recognition. 2019, p. 4690–9.
[9] Kola DGR, Samayamantula SK. A novel approach for facial expression recognition using local binary pattern with adaptive window. Multimedia Tools Appl 2021;80:2243–62.
[10] Oloyede MO, Hancke GP, Myburgh HC. A review on face recognition systems: recent approaches and challenges. Multimedia Tools Appl 2020;79:27891–922.
[11] Gattal A, Djeddi C, Bensefia A, Ennaji A. Handwriting based gender classification using cold and hinge features. In: Image and signal processing: 9th international conference, ICISP 2020, marrakesh, Morocco, June 4–6, 2020, proceedings 9. Springer; 2020, p. 233–42.
[12] Wu Q, Guo G, et al. Gender recognition from unconstrained and articulated human body. Sci World J 2014;2014.
[13] Zeng Y-M, Wu Z-Y, Falk T, Chan W-Y. Robust GMM based gender classification using pitch and RASTA-PLP parameters of speech. In: 2006 international conference on machine learning and cybernetics. IEEE; 2006, p. 3376–9.
[14] Kotti M, Kotropoulos C. Gender classification in two emotional speech databases. In: 2008 19th international conference on pattern recognition. IEEE; 2008, p. 1–4.
[15] Meena K, Subramaniam KR, Gomathy M. Gender classification in speech recognition using fuzzy logic and neural network. Int Arab J Inf Technol 2013;10(5):477–85.
[16] SEDAGHI M. A comparative study of gender and age classification in speech signals. Iran J Electr Electron Eng 2009.

[17] Sánchez-Hevia HA, Gil-Pita R, Utrilla-Manso M, Rosa-Zurera M. Age group classification and gender recognition from speech with temporal convolutional neural networks. Multimedia Tools Appl 2022;81(3):3535–52.
[18] Yücesoy E. Speaker age and gender classification using GMM supervector and NAP channel compensation method. J Ambient Intell Humaniz Comput 2022;13(7):3633–42.
[19] Xu C, Makihara Y, Liao R, Niitsuma H, Li X, Yagi Y, Lu J. Real-time gait-based age estimation and gender classification from a single image. In: Proceedings of the IEEE/CVF winter conference on applications of computer vision. 2021, p. 3460–70.
[20] Sabir AT, Maghdid HS, Asaad SM, Ahmed MH, Asaad AT. Gait-based gender classification using smartphone accelerometer sensor. In: 2019 5th international conference on frontiers of signal processing. ICFSP, IEEE; 2019, p. 12–20.
[21] Patua R, Muchhal T, Basu S. Gait-based person identification, gender classification, and age estimation: a review. In: Progress in advanced computing and intelligent engineering: proceedings of ICACIE 2019. vol. 1, Springer; 2021, p. 62–74.
[22] Isaac ER, Elias S, Rajagopalan S, Easwarakumar K. Multiview gait-based gender classification through pose-based voting. Pattern Recognit Lett 2019;126:41–50.
[23] Harris EJ, Khoo I-H, Demircan E. A survey of human gait-based artificial intelligence applications. Front Robot AI 2022;8:749274.
[24] Deligianni F, Guo Y, Yang G-Z. From emotions to mood disorders: A survey on gait analysis methodology. IEEE J Biomed Heal Inform 2019;23(6):2302–16.
[25] Azhar M, Ullah S, Raees M, Rahman KU, Rehman IU. A real-time multi view gait-based automatic gender classification system using kinect sensor. Multimedia Tools Appl 2023;82(8):11993–2016.
[26] Azhar M, Ullah S, Ullah K, Syed I, Choi J. A gait-based real-time gender classification system using whole body joints. Sens 2022;22(23):9113.
[27] Goshvarpour A, Goshvarpour A. EEG spectral powers and source localization in depressing, sad, and fun music videos focusing on gender differences. Cogn Neurodynamics 2019;13:161–73.
[28] Jun K, Oh S, Lee S, Lee D-W, Kim MS. Automatic pathological gait recognition by a mobile robot using ultrawideband-based localization and a depth camera. In: 2022 31st IEEE international conference on robot and human interactive communication. RO-MAN, IEEE; 2022, p. 652–9.
[29] Rana SP, Dey M, Ghavami M, Dudley S. Non-contact human gait identification through IR-UWB edge-based monitoring sensor. IEEE Sens J 2019;19(20):9282–93.
[30] Anderson B, Shi M, Tan VY, Wang Y. Mobile gait analysis using foot-mounted UWB sensors. Proc ACM Interact Mob Wearable Ubiquitous Technol 2019;3(3):1–22.
[31] Rana SP, Dey M, Ghavami M, Dudley S. Markerless gait classification employing 3D IR-UWB physiological motion sensing. IEEE Sens J 2022;22(7):6931–41.
[32] Arra A, Bianchini A, Chavez J, Ciravolo P, Nebiu F, Olivelli M, Scoma G, Tavoletta S, Zagaglia M, Vecchio A. Personalized gait-based authentication using UWB wearable devices. In: Proceedings of the 27th ACM conference on user modeling, adaptation and personalization. 2019, p. 206–10.
[33] di Biase L, Pecoraro PM, Pecoraro G, Caminiti ML, Di Lazzaro V. Markerless radio frequency indoor monitoring for telemedicine: gait analysis, indoor positioning, fall detection, tremor analysis, vital signs and sleep monitoring. Sens 2022;22(21):8486.
[34] Rana SP, Dey M, Ghavami M, Dudley S. 3-D gait abnormality detection employing contactless IR-UWB sensing phenomenon. IEEE Trans Instrum Meas 2021;70:1–10.
[35] Rana SP, Dey M, Ghavami M, Dudley S. ITERATOR: A 3D gait identification from IR-UWB technology. In: 2019 41st annual international conference of the IEEE engineering in medicine and biology society. EMBC, IEEE; 2019, p. 782–7.
[36] You M, Jiang T. A method of obstacle identification based on UWB and selected bispectra. In: Communications, signal processing, and systems: the 2012 proceedings of the international conference on communications, signal processing, and systems. Springer; 2012, p. 373–82.
[37] Liu T, Ye X, Sun B. Combining convolutional neural network and support vector machine for gait-based gender recognition. In: 2018 Chinese automation congress. CAC, IEEE; 2018, p. 3477–81.
[38] Hassan OMS, Abdulazeez AM, TİRYAKİ VM. Gait-based human gender classification using lifting 5/3 wavelet and principal component analysis. In: 2018 international conference on advanced science and engineering. ICOASE, IEEE; 2018, p. 173–8.
[39] Jain A, Kanhangad V. Gender classification in smartphones using gait information. Expert Syst Appl 2018;93:257–66.
[40] Nutakki C, Edakkepravan H, Gunasekaran S, Ramachandran LP, Sasi V, Nair B, Diwakar S. Torque analysis of male-female gait and identification using machine learning. In: 2018 international conference on advances in computing, communications and informatics. ICACCI, IEEE; 2018, p. 2103–6.
[41] Khabir KM, Siraj MS, Ahmed M, Ahmed MU. Prediction of gender and age from inertial sensor-based gait dataset. In: 2019 joint 8th international conference on informatics, electronics & vision (ICIEV) and 2019 3rd international conference on imaging, vision & pattern recognition. icIVPR, IEEE; 2019, p. 371–6.
[42] Ni Z, Huang B. Human identification based on natural gait micro-Doppler signatures using deep transfer learning. IET Radar Sonar Navig 2020;14(10):1640–6.
[43] Saleem AA, Siddiqui HUR, Sehar R, Dudley S. Gender classification based on gait analysis using ultrawide band radar augmented with artificial intelligence. Expert Syst Appl 2024;249:123843.
[44] Wazzeh A, Birdal RG, Sertbaş A. Human gait based gender detection using light CNN with max feature map. In: 2019 4th international conference on computer science and engineering. UBMK, IEEE; 2019, p. 1–4.
[45] Huang B, Luo Y, Xie J, Pan J, Zhou C. Attention-aware spatio-temporal learning for multi-view gait-based age estimation and gender classification. IET Comput Vis 2022.
[46] Lau L, Chan K. Tree structure convolutional neural networks for gait-based gender and age classification. Multimedia Tools Appl 2023;82(2):2145–64.
[47] Mawlood ZQ, Sabir AT. Human gait-based gender classification using neutral and non-neutral gait sequences. Innovaciencia 2019;7(1):1–13.
[48] Taylor JD. Introduction to ultra-wideband radar systems. CRC Press; 2020.
[49] Frothingham S. Stride length and step length. 2018, Medically reviewed by Daniel Bubnis, M.S., NASM-CPT, NASE Level II-CSS, Fitness. URL: https://www.healthline.com/health/stride-length.
[50] Lalitha S, Mudupu A, Nandyala BV, Munagala R. Speech emotion recognition using DWT. In: 2015 IEEE international conference on computational intelligence and computing research. ICCIC, IEEE; 2015, p. 1–4.
[51] Yantorno RE, Krishnamachari KR, Lovekin JM, Benincasa DS, Wenndt SJ. The spectral autocorrelation peak valley ratio (sapvr)-a usable speech measure employed as a co-channel detection system. In: Proceedings of IEEE international workshop on intelligent signal processing. WISP, vol. 21, 2001.
[52] Siddiqui H-U-R, Raza A, Saleem AA, Rustam F, Díez IdlT, Aray DG, Lipari V, Ashraf I, Dudley S. An approach to detect chronic obstructive pulmonary disease using UWB radar-based temporal and spectral features. Diagn 2023;13(6):1096.
[53] Tamarit L, Goudbeek M, Scherer K. Spectral slope measurements in emotionally expressive speech. Proc Speech Anal Process Knowl Discov 2008;169–83.
[54] Siddiqui HUR, Zafar K, Saleem AA, Raza MA, Dudley S, Rustam F, Ashraf I. Emotion classification using temporal and spectral features from IR-UWB-based respiration data. Multimedia Tools Appl 2023;82(12):18565–83.
[55] Hosseinzadeh D, Krishnan S. Combining vocal source and MFCC features for enhanced speaker recognition performance using GMMs. In: 2007 IEEE 9th workshop on multimedia signal processing. IEEE; 2007, p. 365–8.
[56] Antoni J. The spectral kurtosis: a useful tool for characterising non-stationary signals. Mech Syst Signal Process 2006;20(2):282–307.
[57] Krishna SR, Rajeswara R, Vizianagaram V. SVM based emotion recognition using spectral features and PCA. Int J Pure Appl Math 2017;114(9):227–35.
[58] Mowla N, Chowdhury SR, Chowdhury TA, Mowla MN, Mahzabeen F. Classification precision in endodontic imaging: Advanced deep learning with adaptive squeeze-and-excitation in enhanced VGG-19 and feature pyramid network. In: TENCON 2024 - 2024 IEEE region 10 conference. TENCON, 2024, p. 1724–8. http://dx.doi.org/10.1109/TENCON61640.2024.10902874.